Chemical Engineering Journal 152 (2009) 406–414

Contents lists available at ScienceDirect

Chemical Engineering Journal

journal homepage: www.elsevier.com/locate/cej

pH-mediated interfacial chemistry and particle interactions in aqueous muscovite dispersions

Ataollah Nosrati, Jonas Addai-Mensah*, William Skinner

Ian Wark Research Institute, University of South Australia, Mawson Lakes, Adelaide, SA 5095, Australia

ARTICLE INFO

Article history:
Received 3 October 2008
Received in revised form 23 April 2009
Accepted 1 May 2009

Keywords:
Clay minerals
Muscovite dispersions
Interfacial chemistry
Particle interactions
Rheology
Leaching

ABSTRACT

Interfacial chemistry and particle interactions of aqueous muscovite dispersions have been investigated in the pH range 2–9. Particle zeta potential, reflecting interfacial chemistry, indicated a strong pH-history and solid loading dependency. Pristine particles' zeta potentials measured from high to low pH indicated an isoelectric point (iep) at ~pH 4.5. Subsequent measurements from low to high pH showed differing electrokinetic potentials with iep shift to higher pH values, the extent of which depended upon particle volume fraction and aging time. Dispersion shear yield stress analysis revealed similar pH-history and solid loading dependency. Incongruent leaching was observed to be responsible for the interfacial chemistry change and rheological behaviour. Upon decreasing pH from 9 to 2, considerable leaching of the key elements in muscovite, Al(III), Si(IV), K^+ and Fe(III), occurred. The species concentrations decreased dramatically upon subsequent pH increase to higher values due to their hydrolysis and specific adsorption. Dispersion shear yield stresses recorded from high to low pH sweep were pH-independent. Similar measurements from low to high pH values, however, showed a strong pH-dependency, with maximum yield values at the ieps. The interfacial chemistry and particle interactions, both displaying bifurcation behaviour, showed good compliance with DLVO theory.

1. Introduction

Due to their ubiquitous nature, clay minerals exert significant influence in a number of hydrometallurgical processing operations including uranium and copper leaching [1], precipitation and waste tailings dewatering [2–4]. The association of clay minerals such as muscovite with other ore phases as middling or liberated particles invariably presents intractable challenges which have a striking impact on concentrated mineral dispersions' particle interactions, flow behaviour, flotability, "pumpability", filtration and thickening processes, etc. Muscovite (ideally, $KAl_2(AlSi_3O_{10})(OH)_2$), sometimes referred to as sericite, is one of the layered mica group clay minerals with a 2:1 structure. The crystal structure comprises an Al–O–Al octahedral (O) layer sandwiched between two Si–O–Al tetrahedral (T) layers. Substitutions of lattice Si^{4+} by Al^{3+} in the tetrahedral layer and Fe^{3+} or Mg^{2+} and Ca^{2+} for Al^{3+} in the octahedral layer which invariably occur, results in a permanent net negative charge on the basal surfaces. The charge deficiency is compensated for by interlayer cations such as K^+ and Na^+ adsorbed between the TOT sheets, fitting closely into the hexagonal holes of the Si–O–Al sheet. The interlayer cations (e.g. K^+) strengthen the bonding between basal planes of TOT sheets, which are normally held by attractive van der Waals forces, through the attractive electrostatic interactions [5]. These forces, consequently, render muscovite particles non-swelling in aqueous environments. Muscovite acquires hydrophilic character as a result of the aluminol groups (–AlOH) exposed at its edge surfaces. Despite the fact that muscovite is widely used in electronics and industrial applications, in the mining and minerals industry, it constitutes a non-valuable gangue mineral when associated with other desired minerals of higher economic value (e.g. copper, gold, uranium and platinum group).

During clay minerals processing in aqueous media at a given pH, the particle size, shape and surface characteristics together with the presence of hydrolysable metal ions play a pivotal role in defining the overall particle interactions in the dispersions [2,3]. The interplay between interfacial chemistry and mineral particles interactions in regulating the net interactions energy potential and hence, colloid stability and rheology at certain pulp pH values has been widely investigated [2–14]. To date however, there is still a dearth of knowledge and understanding of the nature of the interfacial chemistry and particle interactions displayed by concentrated dispersions of the various isomorphously substituted mica group clay minerals such as muscovite, under certain industrially relevant processing conditions. For a given pH and temperature ranges, whether or not a given muscovite clay dispersion displays shear thinning or thickening behaviour, is not predictable from the pristine particle surface chemistry, solution speciation and supernate

* Corresponding author. Tel.: +61 8 8302 3673; fax: +61 8 8302 3683.
E-mail address: jonas.addai-mensah@unisa.edu.au (J. Addai-Mensah).

1385-8947/$ – see front matter © 2009 Elsevier B.V. All rights reserved.
doi:10.1016/j.cej.2009.05.001

ionic strength. As muscovite may leach or dissolve in an aqueous environment, pH- dependent hydrolytic and oxolation reactions of dissolved products (e.g. Al(III), Fe(III), Si(IV)) and their subsequent adsorption and precipitation onto particles' surface can significantly change the underlying interfacial properties [14]. Under certain processing conditions, the prevailing clay pulp chemistry and particle interactions may lead to unexpected, intractable rheological (e.g. high yield stress) issues and dewaterability challenges [2–4].

Of particular interest in the present work is the influence of pH-mediated pulp interfacial chemistry on particle interactions prevailing in dilute and concentrated (8–65 wt.% solid or 0.03–0.4 volume fraction), aqueous dispersions of muscovite at pH range 2–11. Specifically, the effect of pH and its history, multivalent metal ions which leach into the supernatant and aging time on interfacial chemistry and rheology is systematically investigated at 25 °C. To quantify the interfacial chemistry, particle zeta potential measurements were conducted at different pH values. The concomitant particle interactions were characterised via dispersion flow curves and shear yield stress measurements. The properties and behaviour of the muscovite investigated herein are pivotal to a number of separation processes in the minerals industry, including hydrometallurgical value mineral (e.g. uranium, gold and copper) extraction, leach and flotation tails dewatering and environmental waste minimization.

2. Experimental methods

2.1. Materials

Polydispersed muscovite particles (Geological Specimen Supplies, Australia) were used in this work as received. The particle BET surface area was 12.7 m^2/g and the 10th, 50th and 90th percentile particle sizes, D_{10}, D_{50} and D_{90}, determined by laser diffraction (Malvern Mastersizer X, Malvern, UK) were 3, 30 and 140 μm, respectively. X-ray powder diffraction confirmed the high crystallinity of the sample whilst XRF analysis showed the oxide components to be SiO_2 (47%), Al_2O_3 (31.8%), K_2O (10%) and Fe_2O_3 (3.6%) and Mn, Mg and Ca as trace elements. Electron microprobe (CAMECA SX51) analysis confirmed $K_{0.91}Na_{0.07}(Al_{1.82}Fe^{3+}_{0.14}Mg_{0.08})(Al_{0.93}Si_{3.07}O_{10})(OH)_2$ to be the exact crystal structure. Dispersions with different solid contents (8–65 wt.%) were used. They were prepared by adding a known mass of dry muscovite particles to a known mass of 10^{-3} M KNO_3 solution used as background electrolyte. Concentrated KOH (Chem-Supply) and HNO_3 (Scharlau Chemie) were used to control and adjust the pH of fresh dispersions during zeta potential and shear yield stress measurements. Dispersions were homogenized by mixing for 10 min using overhead stirrer at 600 rpm before altering pH. High purity Milli-Q water (specific conductivity < 0.5 μS cm^{-1}, surface tension at 20 °C of 72.8 mN m^{-1} and pH of 5.6) was used for preparation of all solutions and dispersions.

2.2. Zeta potential measurements

For interfacial chemistry characterization, the zeta potential of particles in low (8 wt.%) and high (50–57 wt.%) solid content dispersions were determined with an Acoustosizer II (Colloidal Dynamics Inc., Australia). This instrument measures the electrokinetic sonic amplitude (ESA) of particles in dispersion and converts it to dynamic mobility. The zeta potential was then determined from the dynamic mobility using the Smoluchowski model [15]. Fresh dispersions were made and their pH decreased from high (~9) to low (~2) and the zeta potential measured at different pH values. For each new pH value, the samples were allowed to equilibrate for 5 min prior to data acquisition.

2.3. Rheological measurements

For rheological studies, dispersions with solid contents in the range of 50–65 wt.% were used. Flow curves and low shear yield stress values (<20 Pa) for dispersions were determined using a couette concentric rheometer (Haake RV1), whilst the higher shear yield stresses (>20 Pa) were measured by the vane technique (Haake VT550). The advantage of the latter technique is the minimised slip between the sample and the instrument fixture [16,17], giving a more accurate yield value particularly for structured dispersions (shear yield stress >20 Pa) [18–20]. For indirect shear yield stress measurements, the shear rate was increased from 0 to 1000 s^{-1} and back to 0 over a 200 s period while shear stress measured continuously as a function of shear rate. As the dispersions showed a non-Newtonian, Bingham plastic behaviour, the shear yield stresses were estimated by extrapolation of the linear part of the flow curves using the Bingham plastic model:

$$\tau = \tau_B + \eta_B \dot{\gamma} \quad (1)$$

where τ and τ_B are the shear stress and Bingham shear yield stress (Pa), respectively, η_P is the plastic viscosity (Pa s) and $\dot{\gamma}$ is the shear rate (s^{-1}). For direct yield stress measurements, the vane was immersed in 0.2 dm^3 dispersion and rotated at constant slow rate (γ = 0.021 s^{-1}) and the yield stress estimated from the maximum torque (T_m) attained using following equation:

$$T_m = \frac{\pi D^3}{2}\left(\frac{H}{D} + \frac{1}{3}\right)\tau_y \quad (2)$$

where D and H are the vane diameter and height (m), respectively and the units of T_m and τ_y are N m and Pa, respectively. To investigate the compliance of the particles interactions with DLVO theory [21,22], the elastic floc model [23,24] was applied on the basis that a linear relation between measured shear yield stress and square of zeta potential will be observed if DLVO forces were dominant:

$$\tau_y = \frac{1}{20 r \eta_s \dot{\gamma}}\left(\frac{A_h}{12 d_1^2} + B(d_1)\zeta^2\right) \quad (3)$$

where τ_y (or τ_B) is shear yield stress (Pa), A_h is Hamaker constant (J), $\dot{\gamma}$ is the shear rate, d_1 is interparticle separation distant (m), r is the particle radius (m), η_s is the suspension viscosity (Pa s), $B(d_1)$ is a fitting constant which is negative in value and dependent on the elasticity of the interparticle bonds and ζ is the particle zeta potential (V).

2.4. Aging behaviour

Dispersions with 8 and 57 wt.% solid contents were prepared and their pH decreased from the pristine value (~pH 9) to pH 2 or 3 and then increased to the initial value after a fixed period of aging (5 min or 1 h). Both the particle zeta potential and shear yield stress of the dispersion were recorded at selected pH values. At each pH unit, dispersions were allowed to equilibrate for 5 min before the measurements were performed and an aliquot of suspension taken for solid-supernatant separation by centrifugation. The resulting supernatants were analysed by inductively coupled plasma (ICP) for speciation. To achieve good reproducibility of results, all rheological, zeta potential and aging measurements were replicated at least three times and the pure errors determined and reported at 95% confidence interval.

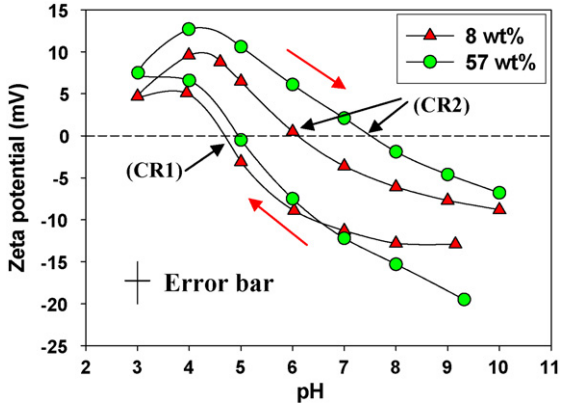

Fig. 1. Particle zeta potential of 8 and 57 wt.% solid muscovite dispersions in 10^{-3} M KNO_3 as a function of pH solution. The arrows indicate the direction of pH sweep.

3. Results and discussion

3.1. Zeta potential and dissolution

Particle zeta potential of 8 wt.% (0.03 vol. fraction) and 57 wt.% (0.03 vol. fraction) solid dispersions as a function of pH in 10^{-3} M KNO_3 solution was measured by first decreasing the pH from ~pH 9 to 3 and then systematically back to pH 10 are shown in Fig. 1. The data show that the electrokinetic potentials were negative in the neutral to alkaline pH range, the magnitude of which was fairly low and, decreased with decreasing pH. An isoelectric point (iep) or first point of charge reversal (CR1) is indicated at ~pH 4.5, which is in good agreement with reported data [25]. Upon a further decrease of pH, the particles become positively charged. The zeta potential and iep for both 8 and 57 wt.% solid dispersions are substantially the same for pH change from 9 to 3. The initial negative electrokinetic potential of the particles is largely attributed to the permanent, negative charge of the isomorphously substituted clay mineral basal faces [14,15,26], and the deprotonated silanol and aluminol groups at the pH-dependent edge faces. Decreasing the pH from 9 to 3, particle surface protonation, mainly of the edge surface hydroxyl groups, occurs [15] and hence, the magnitude of negative electrokinetic potential of the particles decreased.

In return pH sweep, as the dispersion pH was raised from 3 to 10, the particles displayed significantly different zeta potentials. This reflected in a bifurcation and noticeable shift of the iep to a higher pH value (CR2). The magnitude of zeta potential first increased to a maximum at pH 4–4.5, before decreasing monotonically with increasing pH. Furthermore, the extent of the pH-mediated electrokinetic potential change is noted to be dispersion solid content dependent. The higher the solid volume fraction the greater the bifurcation effect and larger iep shift to higher pH. These observations are in good agreement with previous studies [4,14,27] and suggest that an irreversible interfacial phenomena were occurring at the particle–solution interface. This behaviour may be ascribed to the effect of multivalent metal ions (e.g. Al(III)) leaching in the acidic pH range, subsequent hydrolysis and specific adsorption onto the surfaces of the muscovite particles with increasing pH [4,14,27,28].

Complementary solution speciation analysis performed at various pH values, confirmed the presence and disappearance of dissolved Al(III), Si(IV) and Fe(III) ions with decreasing and increasing dispersion pH, respectively (Figs. 2 and 3). These data also show significant leaching of K^+ ions with decreasing pH. However, since KOH solution was used to increase the dispersion pH, exact trend followed by the concentration of K^+ ions could not be deconvoluted with increasing pH. The use of NaOH to modify the pH and assess the behaviour of the K^+ ions with pH increase from 3 to 10 is currently under investigation.

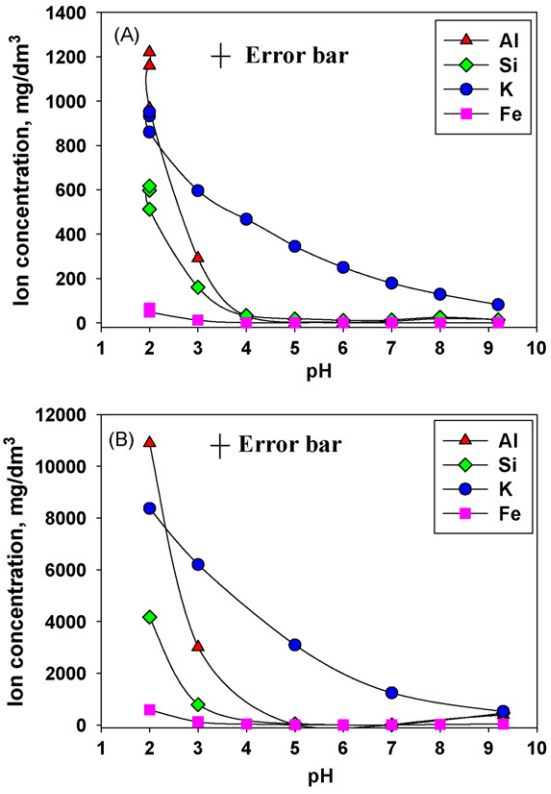

Fig. 2. Concentration of Al(III), Si(IV), Fe(III) and K ions leached into solution from muscovite dispersions in 10^{-3} M KNO_3, measured with ICP. For both 8 wt.% (A) and 57 wt.% solid (B) dispersions the pH decreased from ~9 to 2.

Fig. 2(A) and (B) suggests that the concentrations of the main constituent elements in muscovite particles that leached were substantially proportional to the pulp solid content. Upon increasing of solid content from 8 to 57 wt.%, the concentration of leached species increased by ~8 times. For the 8 wt.% solid dispersions (A) at pH 2, the pulp was allowed to age 1 h longer before increasing the pH. The resulting data points are indicated as the two highest concentrations (at pH 2), indicating that the dissolution rate after an initially fast regime was practically insignificant over a longer time. The data also suggest that above pH 3, the leach of interlayer K^+ ions from the muscovite structure occurs more readily in comparison with the covalently bonded Al(III) and Si(IV) lattice ions. Furthermore, significant variation is observed in the elemental concentrations with pH, in particular between Al(III) and Si(IV) which have quite similar atomic concentrations in the initial crystal lattice. The maximum, molar concentrations of Al(III), Si(IV) and Fe(III) species observed at pH 2 are 4.44×10^{-2}, 2.14×10^{-2} and 1.81×10^{-3} M, respectively, for 8 wt.% solid content and 4.11×10^{-1}, 1.54×10^{-1} and 1.43×10^{-2} M, respectively, for the 57 wt.% solid dispersion. This trend is indicative of incongruent leaching behaviour and highlights the fact that the both the octahedrally and tetrahedrally coordinated lattice Al(III) ions leaches out more rapidly than the tetrahedrally coordinated Si(IV) species [14,29].

The links between pulp chemistry and dispersion's electrokinetic behaviour, specifically the probable reasons for observed bifurcations, were investigated as delineated below. The complete concentrations profile of leached Al(III), Si(IV) and Fe(III) species in the high to low and low to high pH sweeps are shown in Fig. 3 for both 8 wt.% (A and B) and 57 wt.% (C and D) solid dispersions. The data are consistent with the general observation of species leaching from the muscovite particles at low pH, followed by hydrolysis and

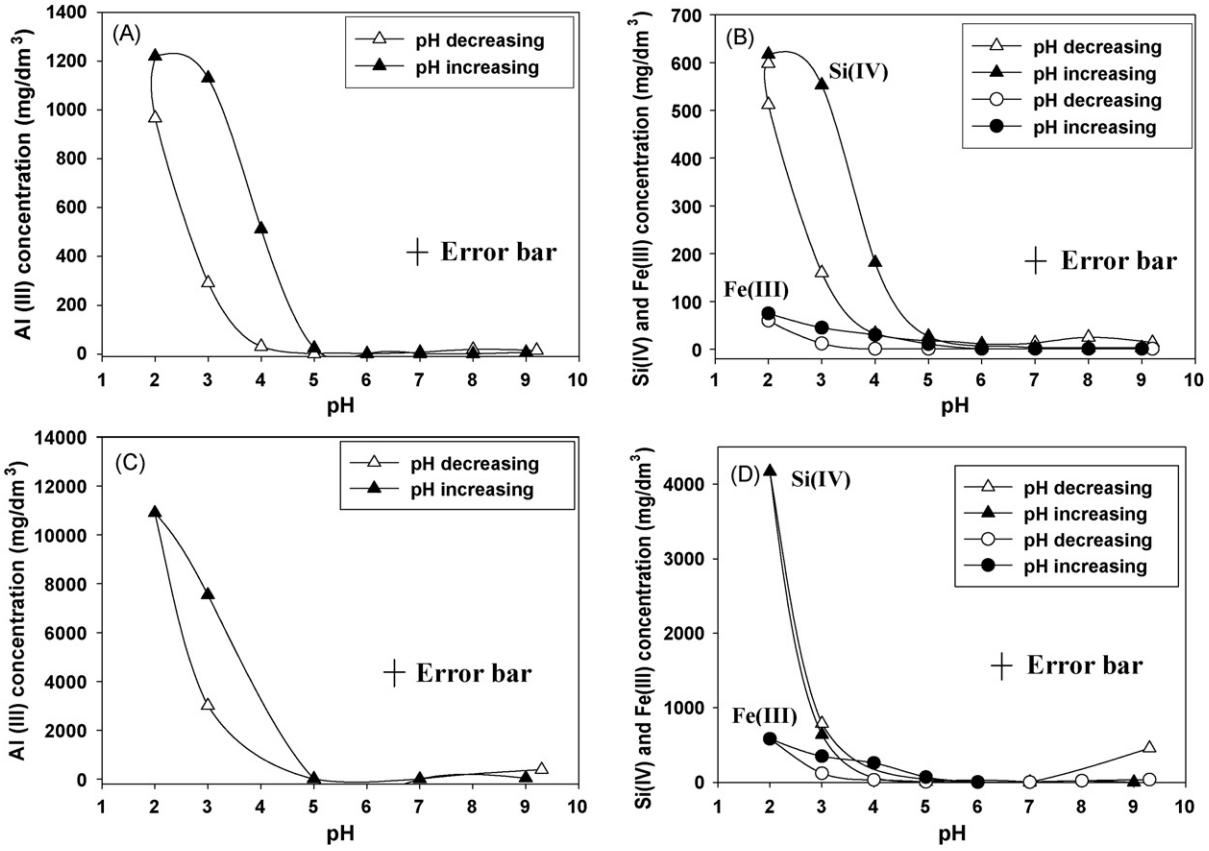

Fig. 3. Concentration of Al(III) and Si(IV) species leached into solution from muscovite dispersions at 8 wt.% (A and B) and 57 wt.% solid (C and D) in 10^{-3} M KNO_3. The dispersion pH was initially decreased from ~9 to 2 and then returned to pH 9.

specific adsorption or even precipitation onto the pulp particles as pH is increased to higher values [14,30–33]. Analysis of the effect of aging time and pH on the zeta potential is presented in Fig. 4 for measurements at pH 2 and 3 with 1 h aging. The results indicate that the lower pH value or the longer aging time at similar low pH value, the greater the impact on particle zeta potential in terms of (i) the magnitude of maximum zeta potential observed at ~pH 4 and (ii) the shift of the second point of charge reversal (CR2). In Fig. 4 it is shown that after 1 h aging at pH 2, the particles display an iep (CR2) similar to that of gibbsite ($Al(OH)_3$). To completely elucidate the trends displayed in Fig. 4, the data in Fig. 3(A) and (B) must be reconciled with pH-speciation changes described in Figs. 5–7.

The equilibrium solubility, calculated speciation and hydrolysis products of Al(III), Si(IV) and Fe(III) ions are shown in Figs. 5–7, respectively. The calculations were based on the principal hydrolysis reactions and products detailed in Table 1, using the reported solubility and hydrolysis constants [30]. Figs. 5A, 6A and 7A predict that the equilibrium solubility of either Al(III), or Si(IV) and Fe(III) species due to the solid phases indicated increase exponen-

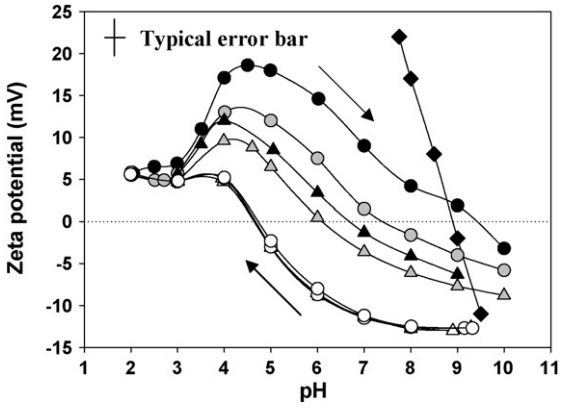

Fig. 4. Particle zeta potential of 8 wt.% muscovite dispersions in 10^{-3} M KNO_3 as a function of pH and aging time. pH was decreased from 9.3 to 3 (5 min aging (△), and aged for 1 h at pH 3 (▲)) and from 9 to 2 (5 min aging (○), and aged for 1 h at pH 2 (●)) and then all returned to 10 (as indicated by the arrows). The unfilled symbols represent the same samples during forward pH sweep from high to low pH. Diamonds (♦) show the zeta potential for pure gibbsite in pH range 7.5–9.5.

Table 1
Principal hydrolysis reactions, products and stability constants for Al(III), Si(IV) and Fe(III) ions.

Aqueous Al(III), Si(IV) and Fe(III) speciation	K	$\log_{10} K$
$Al(OH)_3(s) + 3H^+ \leftrightarrow Al^{3+} + 3H_2O$	K_{S0}	9.58
$Al^{3+} + H_2O \leftrightarrow Al(OH)^{2+} + H^+$	$K_{1,1}$	−5.47
$Al^{3+} + 2H_2O \leftrightarrow Al(OH)_2^+ + 2H^+$	$K_{1,2}$	−10.28
$Al^{3+} + 3H_2O \leftrightarrow Al(OH)_3 + 3H^+$	$K_{1,3}$	−16.08
$Al^{3+} + 4H_2O \leftrightarrow Al(OH)_4^- + 4H^+$	$K_{1,4}$	−23.66
$2Al^{3+} + 2H_2O \leftrightarrow Al_2(OH)_2^{4+} + 2H^+$	$K_{2,2}$	−7.7
$3Al^{3+} + 4H_2O \leftrightarrow Al_3(OH)_4^{5+} + 4H^+$	$K_{3,4}$	−13.43
$13Al^{3+} + 28H_2O \leftrightarrow Al_{13}O_4(OH)_{24}^{7+} + 32H^+$	$K_{13,24}$	−104.38
$SiO_2(s, quartz) + 2H_2O \leftrightarrow Si(OH)_4$	K_{S0}	−4
$Si(OH)_4(aq) \leftrightarrow SiO(OH)_3^- + H^+$	$K_{1,1}$	−9.21
$Si(OH)_4(aq) \leftrightarrow SiO_2(OH)_2^{2-} + 2H^+$	$K_{1,2}$	−20.97
$4Si(OH)_4(aq) \leftrightarrow Si_4O_6(OH)_6^{2-} + 4H_2O + 2H^+$	$K_{4,2}$	−11.12
$4Si(OH)_4(aq) \leftrightarrow Si_4O_8(OH)_4^{4-} + 4H_2O + 4H^+$	$K_{4,4}$	−29.32
α-$FeO(OH)(s) + 3H^+ + H_2O \leftrightarrow Fe^{3+} + 3H_2O$	K_{S0}	1.173
$Fe^{3+} + H_2O \leftrightarrow Fe(OH)^{2+} + H^+$	$K_{1,1}$	−2.77
$Fe^{3+} + 2H_2O \leftrightarrow Fe(OH)_2^+ + 2H^+$	$K_{1,2}$	−6.42
$Fe^{3+} + 3H_2O \leftrightarrow Fe(OH)_3 + 3H^+$	$K_{1,3}$	−12.67
$Fe^{3+} + 4H_2O \leftrightarrow Fe(OH)_4^- + 4H^+$	$K_{1,4}$	−21.95
$2Fe^{3+} + 2H_2O \leftrightarrow Fe_2(OH)_2^{4+} + 2H^+$	$K_{2,2}$	−2.63
$3Fe^{3+} + 4H_2O \leftrightarrow Fe_3(OH)_4^{5+} + 4H^+$	$K_{3,4}$	−5.79

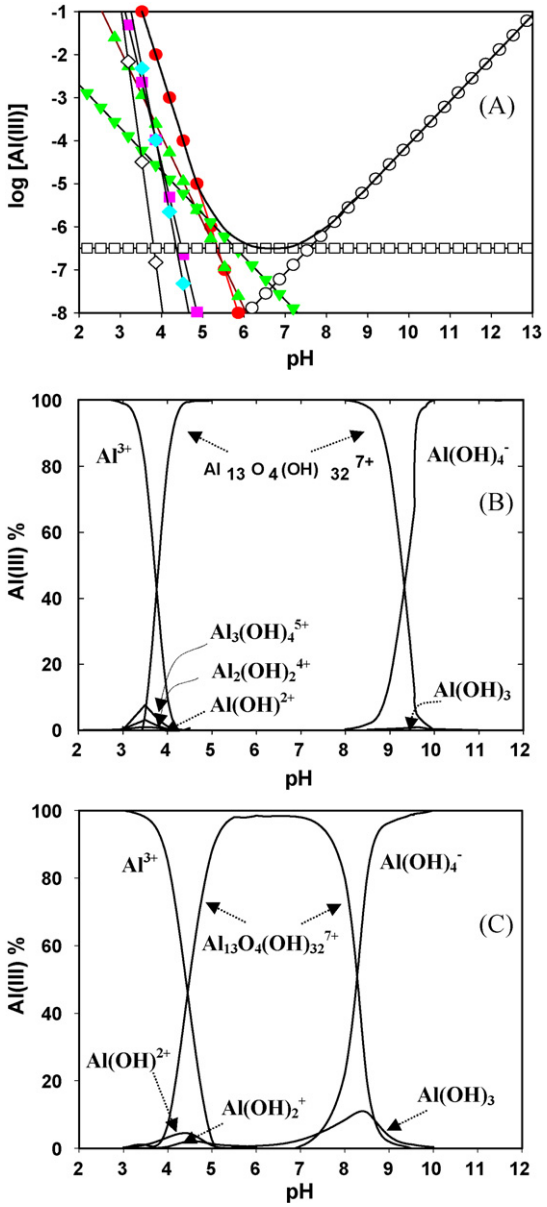

Fig. 5. Calculated equilibrium solubility and speciation (A) and fractional abundance in (B) 0.1 M Al(III) and (C) 0.001 M Al(III), with the distribution of various species: Al^{3+} (●), $Al(OH)^{2+}$ (▲), $Al(OH)_2^{+}$ (▼), $Al_2(OH)_2^{4+}$ (■), $Al_3(OH)_4^{5+}$ (◆), $Al_{13}O_4(OH)_{32}^{7+}$ (◊), $Al(OH)_3$ (□), and $Al(OH)_4^{-}$ (○) as a function of pH at I = 1 M and 25 °C; the heavy curve in A is the total concentration of Al(III).

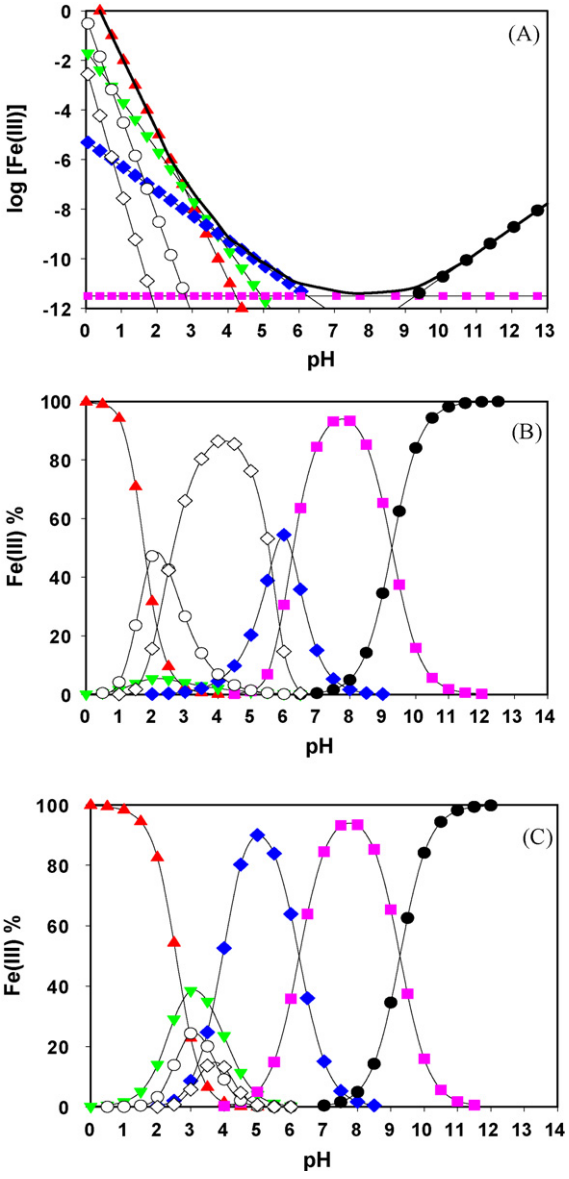

Fig. 6. Calculated equilibrium solubility and speciation (A) and fractional abundance in (B) 0.1 M Fe(III) and (C) 0.001 M Fe(III), with the distribution of various species: Fe^{3+} (▲), $Fe(OH)^{2+}$ (▼), $Fe(OH)_2^{+}$ (◆), $Fe_2(OH)_2^{4+}$ (○), $Fe_3(OH)_4^{5+}$ (◊), $Fe(OH)_3$ (■), and $Fe(OH)_4^{-}$ (●) as a function of pH at I = 1 M and 25 °C; the heavy curve in A is the total concentration of Al(III).

tially with decreasing pH from neutral to acidic values at 25 °C. The solubilities also increase sharply with increasing pH in alkaline solutions. This is in good agreement with the data shown in Fig. 3 where all the dissolved species concentrations increase dramatically with decreasing pH <5. The speciation and distribution of hydrolysis products as a function of pH are shown in Figs. 5–7(B) and (C). The data clearly indicate that, depending upon the total species concentration in solution, Al^{3+} and Fe^{3+} ions may begin to hydrolyse at pH 3–4 and 1–2, respectively. The higher the species ionic strength, the lower the pH at which the hydrolysis begins. For Si(IV) however, monomeric $Si(OH)_4$ species prevail in the pH range 1–6, after which hydrolysis begins (pH 6.5–7.5). The decrease in ionic concentration of Al(III), Si(IV) and Fe(III) with pH increase is consistent with specific adsorption of the individual hydrolysis complexes, and their combinations thereof, onto the surface of the muscovite particles in suspension, as may be predicted from the James and Healy model [28]. The greater the adsorbed electropositive complex coverage is, the larger the shift of the iep (CR2) to higher pH values. The extent of iep shift correlates positively with the maximum particle zeta potential which is observed at pH 4.0–4.5. Both parameters increase monotonically with increasing solution hydrolysable species concentration.

A plethora of electropositive Al(III) and Fe(III) complexes which form at specific pH values together with the $Si(OH)_4$ species may interact and form various complexes in dynamic equilibrium within the pH range 3–7. For instance, the formation of hydroxyaluminosilicates complexes due to polycondensation reactions between the silicic acid and Al(III) species in acidic and alkaline solutions [34], used to produce zeolitic compounds, is well known. Furthermore, the concentration of Al(III), Fe(III) and Si(IV) species in solution leached from muscovite are all indicated to exceed the equilibrium solubilities of pure silica and metal hydroxides displayed in Figs. 5–7(A). Hence, following their hydrolysis

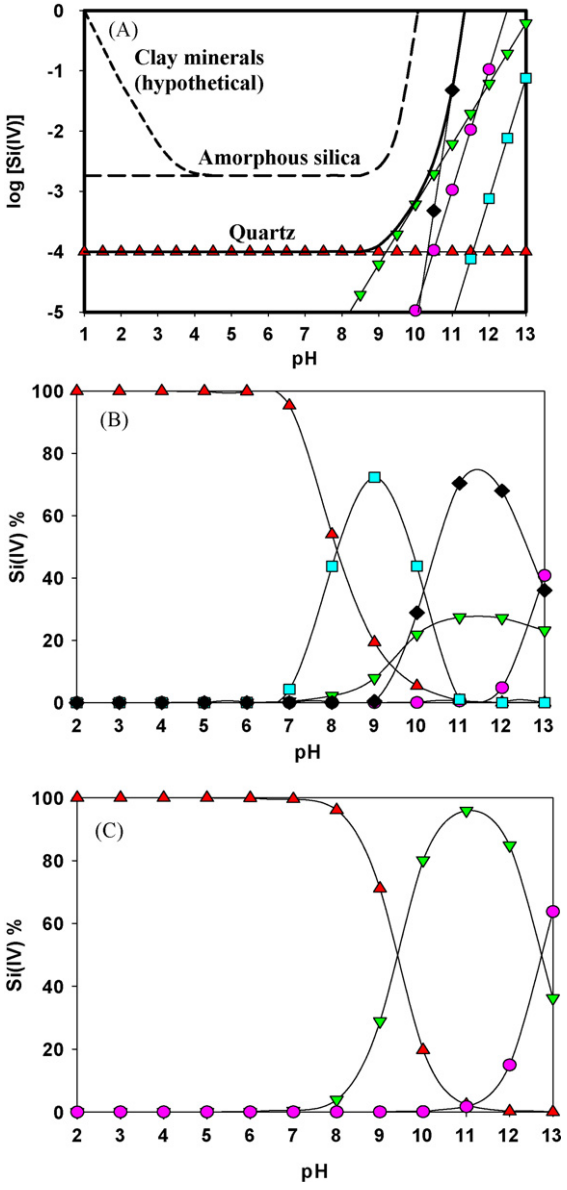

Fig. 7. Calculated equilibrium solubility and speciation (A) and fractional abundance in (B) 0.1 M Si(IV) and (C) 0.001 M Si(IV), with the distribution of various species: $Si(OH)_4$ (▲), $SiO(OH)_2^-$ (▼), $SiO_2(OH)_2^{2-}$ (●), $Si_4O_6(OH)_6^{2-}$ (■) and $Si_4O_8(OH)_4^{4-}$ (♦) as a function of pH at $I = 3$ M and 25 °C.

these supersaturated species are both thermodynamically and kinetically predisposed to adsorb, polycondense, surface nucleated and precipitate as secondary mineral phases at muscovite solid residue surfaces. The reduction in species concentration in solution with pH increase from 2 to 5 concurs with this observation. Optically clear supernatants obtained by centrifugation of slurry samples removed during pH increase from 2 or 3 to 10 produced colloidal precipitates, the amount and colour of which was pH-dependent.

It may be concluded from the systematic shift of the iep to higher pH values upon pH increase that the muscovite particles were coated with Al(III), Si(IV) and Fe(III)-containing surface layers to a differing extent. The greatest iep shift occurring at pH 10 is similar to that of colloidal gibbsite (γ-$Al(OH)_3$) and falls within the reported iep range (pH 9.0–10.5) of gibbsite and alumina (Al_2O_3) [8,31,35]. This, thus, confirms that the interfacial layer was aluminium hydr(oxide) like in character, following intense leaching of muscovite at low pH 2 and subsequent increase of pulp pH to

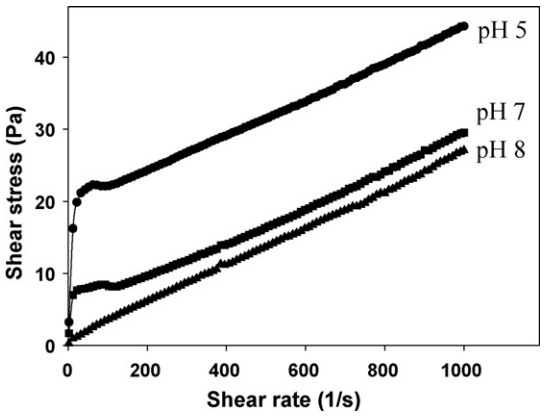

Fig. 8. Typical flow curves of 57 wt.% solid muscovite dispersion in 10^{-3} M KNO_3 at three different pH values.

higher value. The interfacial chemistry and concomitant particle interactions may be probed in the following rheological and zeta potential investigations.

3.2. Particle interactions: rheology

3.2.1. Typical flow curves

Fig. 8 shows the typical flow curves of 57 wt.% solid dispersion at pH 8, 7 and 5 where the particles experiencing high, moderate and no zeta potential, respectively. An approximately Newtonian behaviour is displayed at close to pristine pH (8–9) conditions. However, a non-Newtonian Bingham plastic behaviour is observed as the pH is decreased, the extent of which accentuated with decreasing pH from 8 to 5. This is consistent with electrokinetic potential data at the same pH values, showing the direct effect of particle zeta potential on particle interactions. As the iep is approached, the repulsive electrical double layer interactions are minimized. The predominance of attractive van der Waals forces between the particles leads to the emergence of a yield value upon application of a shear stress.

3.2.2. Effect of pH and solid content

Shear yield stress was measured for muscovite dispersions in 10^{-3} M KNO_3 solution, as a function of pH, solid content and different pH histories (from high to low and then low to high pH). Fig. 9(A) for solid contents in the range 55–65 wt.% (equivalent to 0.03 vol. fraction) indicates a gel point around 60 wt.% above which a step change in particle networking occurs and the pulp structure strength is dramatically amplified. It is observed that when the pH is decreased from 7 to 5 and 3, the dispersions yield stress showed no noticeable change. This observation may, at first, appear to be contrary to the zeta potential data shown in Fig. 1. It may, however, be rationalized in terms of the fact that at these high volume fractions, the subtle variation of the magnitude of particle zeta potentials being $<|10|$ mV due to the pH change, had no significant impact on the overall inter-particle forces which determined the shear yield stress. Subsequent shear yield stress measurements from low to high pH values, on the other hand, revealed strong pH-dependent particle interactions, particularly above the gel point (i.e. >60 wt.% solid). Fig. 9(B) shows that upon increasing 65 wt.% solid dispersions' pH from 3, the yield stress first decreased from a 400 Pa to ~20 Pa at pH 4 and then started to increase systematically to ~130 Pa at pH 5 and reached maximum (~550 Pa) at pH 7 (CR2).

To explain the pH history mediated rheological behaviour exhibited in Fig. 9(B) in a set of shear yield stress and cognate particle zeta potential data for 57 wt.% solid muscovite dispersions as a function of pH are plotted together in Fig. 10. The data clearly indicate that at

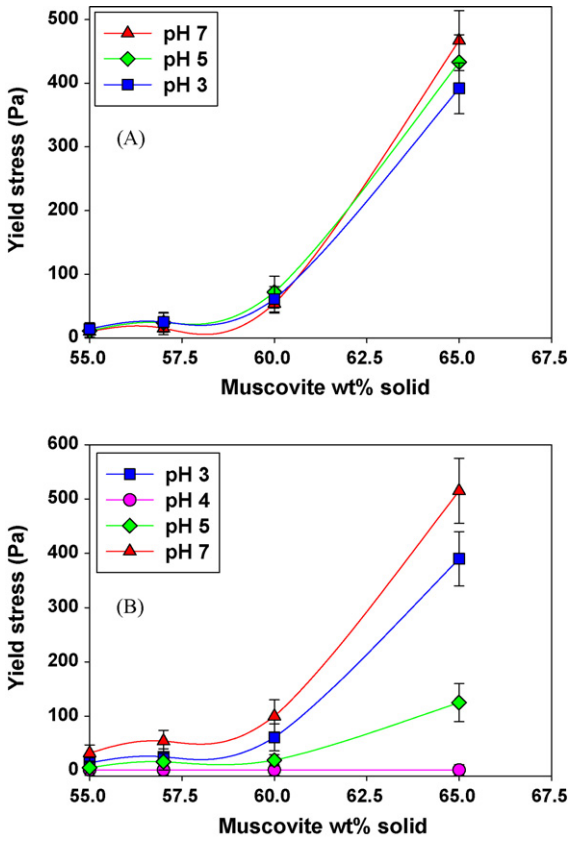

Fig. 9. Shear yield stress as a function of solid content of muscovite dispersion in 10^{-3} M KNO_3 at different pH values. The yield stress was measured from pH 7 to 3 (A) and then from pH 3 to 7 (B).

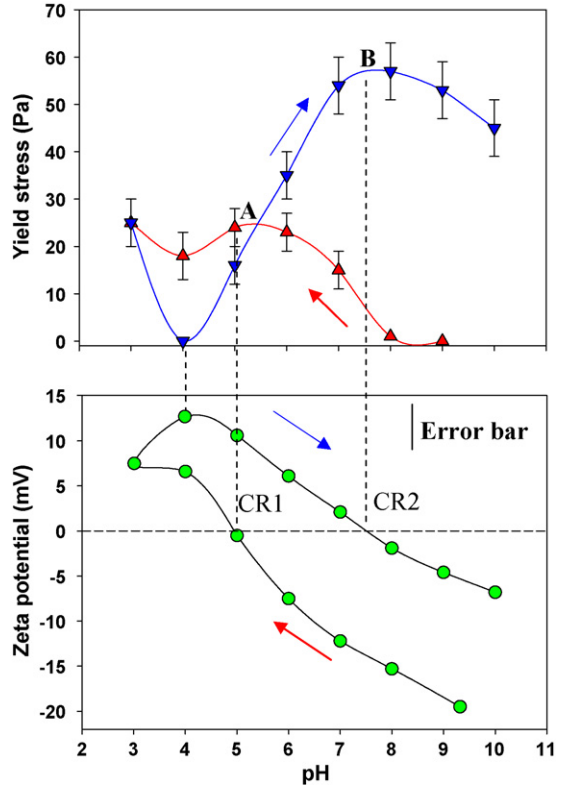

Fig. 10. Shear yield stress (top) and particle zeta potential (bottom) of 57 wt.% solid muscovite dispersion as a function of pH in 10^{-3} M KNO_3 solution. The arrows indicate the direction of pH change.

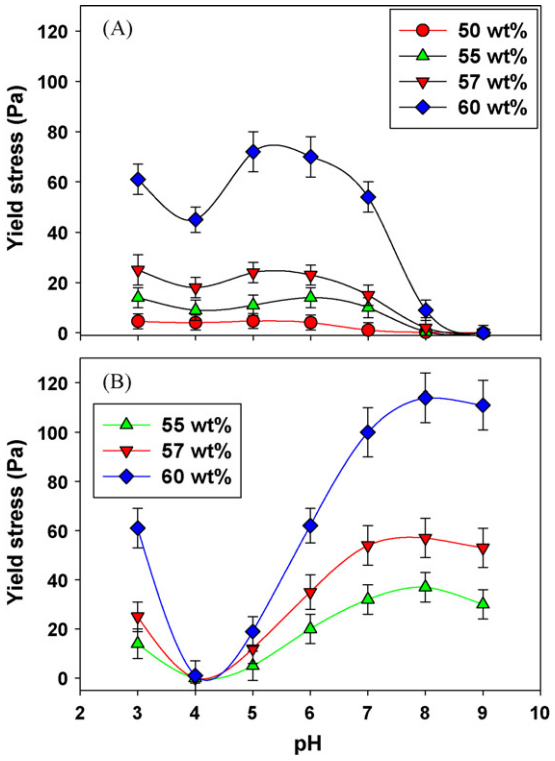

Fig. 11. Shear yield stress as a function of pH for 50 to 60 wt.% solid muscovite dispersions in 10^{-3} M KNO_3 solution. pH first decreased from 9 to 3 (A) and then increased from 3 to 9 (B).

pristine pH (9.2), where zeta potential was −20 mV, the dispersion shows no noticeable yield stress. Upon decreasing the pH, however, the shear yield stress increases systematically to a maximum at around pH 5 (CR1) where the zeta potential is zero. The attractive van der Waals forces start to dominate the particle interactions in the absence of electrostatic repulsive forces at the iep (CR1) [24,36]. Moreover, assuming the iep of edge faces for clay minerals to be around pH 6–7 [37–39], it is likely that by decreasing pH to <6, the edge-face electrostatic repulsive forces diminish and instead some edge-face attractive electrostatic forces may arise and contribute to increased attractive forces. A further decrease of pH results in a small increase in zeta potential with a marginal variation in yield stress.

Fig. 10 also indicates that on subsequent increase of pH from 3 to 10, the yield stress first decreased dramatically to zero at pH 4. Thereafter, it increased gradually and reached maximum value at pH 7–8 (point B). This observation correlates well with the corresponding particle zeta potential data. At pH 4–4.5 the particles acquire maximum positive charge or zeta potential (≈14 mV) due to the specific adsorption of electropositive Al(III), and to some extent Fe(III), complexes arising from leaching at pH 3. Seemingly, the resulting interfacial structure and particles interactions produced strong repulsive forces which reflected low yield stress at pH 4. At pH 8 (CR2) the particles are neutrally charged and attractive van der Waals and also particle bridging by surface nucleation and cementation forces govern the overall particle interactions in the dispersion. Similar pH-history dependent dispersion rheology observed at different solid content (volume fraction) of muscovite dispersions is shown in Fig. 11(A) and (B).

To investigate the compliance of particle interactions with DLVO theory [21,22], further analysis was performed through the application of the elastic floc model (Eq. (3)) [24]. From Fig. 12, the shear yield stress of 57 wt.% muscovite dispersion decreases linearly with increasing zeta potential squared. Clearly, two sets of data emerge

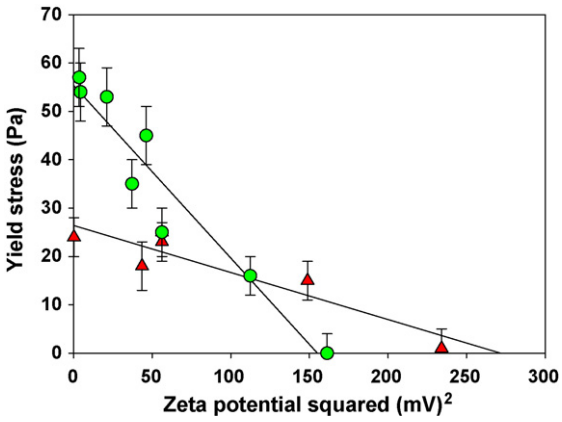

Fig. 12. Shear yield stress as a function of the square of the zeta potential for 57 wt.% solid muscovite dispersion in 10^{-3} M KNO_3 solution. The pH first decreased from 9 to 3 (▲) and then increased from 3 to 10 (●).

as indicated by the straight lines fitted to the pH-sweep data. The observed difference reflects the changes in solution and interfacial chemistry of same dispersion with different pH histories. The data confirms the altered surface chemistry of the muscovite particles due to leaching of Al(III), Si(IV) and Fe(III) species into solution and their subsequent disappearance from the aqueous phase as hydrolysis products or complexes which deposited onto the surface of particles. Assuming no noticeable change in the particles' size due to the formation Al(III)–Si(IV)-rich containing interfacial layer, the different maximum shear yield stresses (intercepts) observed at CR1 and CR2 may suggest a noticeable change in the effective Hamaker constant of particles. Based on literature data [40–45] the ratio of Hamaker constant (in $zJ = 10^{-21}$ J) for alumina (36.7, 67, 21, 33) in water to muscovite (13.4, 22, 7.7 and 11.8) in water is about three times. It is also possible that surface nucleation and precipitation of the supersaturated Al(III)/Si(IV) species at pH 8 (CR2) enhanced the interfacial area of particle contact, facilitating particle bridging by aggregation and cementation. These in tandem with van der Waals forces would account for the significantly higher yield stress observed at CR2 in comparison with CR1.

4. Conclusions

The interfacial chemistry and particle interactions of muscovite dispersions and their variation with pH, solid content and solution speciation have been investigated. The particles zeta potentials and dispersion shear rheology both showed a pH-history dependent behaviour. Significant incongruent leaching of major constituent elements of muscovite (Al(III), Si(IV), Fe(III) and K^+) at acidic pH was implicated, the extent of which increased dramatically by decreasing pH, increasing solid volume fraction and aging time. Hydrolysis and specific adsorption of leached Al(III), Si(IV) and Fe(III) species onto muscovite particles surface upon increasing pH led to the development of a new interfacial layer. These interfacial changes reflected in dramatic modification of particle zeta potential, exemplified by a significant isoelectric point shift that is reminiscent of gibbsite (γ-$Al(OH)_3$) particles surface. The concomitant shear yield stress data showed maximum particle attraction at the different isoelectric points, whilst negligible shear yield stress was displayed where the magnitude of the particles zeta potential was greatest. Clear links between the interfacial chemistry and muscovite particle interactions which show good compliance with the DLVO theory, have emerged. The findings show that pH-mediation of muscovite pulp's interfacial chemistry can be dramatic, with a striking impact on particle interactions and flow behaviour during aqueous processing.

Acknowledgments

Financial support for the project from BHP-Billiton and the Australian Research Council is gratefully acknowledged. A. Nosrati also acknowledges the helpful cooperation from Terry Dermis and useful discussions with John Lawson of BHP-Billiton.

References

[1] S.J. Macnaughton, L. Tan, A. Day, R.J. Ring, Modelling the leaching behaviour of an uranium ore, in: Uranium 2000: International Symposium on the Process, 2000, pp. 413–427.
[2] P. Mpofu, J. Addai-Mensah, J. Ralston, Influence of hydrolyzable metal ions on the interfacial chemistry, particle interactions, and dewatering behavior of kaolinite dispersions, J. Colloid Interface Sci. 261 (2) (2003) 349–359.
[3] J. Addai-Mensah, A.J. McFarlane, K.E. Bremmell, Optimising the dewatering behaviour of clay tailings through interfacial chemistry, orthokinetic flocculation and controlled shear, Powder Technol. 160 (1) (2005) 27–34.
[4] K.E. Bremmell, J. Addai-Mensah, Interfacial-chemistry mediated behavior of colloidal talc dispersions, J. Colloid Interface Sci. 283 (2) (2005) 385–391.
[5] M.L. Schlegel, K.L. Nagy, P. Fenter, L. Cheng, N.C. Sturchio, S.D. Jacobsen, Cation sorption on the muscovite (0 0 1) surface in chloride solutions using high-resolution X-ray reflectivity, Geochim. Cosmochim. Acta 70 (14) (2006) 3549–3565.
[6] K.G. Knauss, T.J. Wolery, Muscovite dissolution kinetics as a function of pH and time at 70 °C, Geochim. Cosmochim. Acta 53 (7) (1989) 1493–1501.
[7] S.B. Johnson, D.R. Dixon, P.J. Scales, The electrokinetic and shear yield stress properties of kaolinite in the presence of aluminium ions, Colloid Surf. A 146 (1–3) (1999) 281–291.
[8] Y.K. Leong, Yield stress and zeta potential of nanoparticulate silica dispersions under the influence of adsorbed hydrolysis products of metal ions—Cu(II), Al(III) and Th(IV), J. Colloid Interface Sci. 292 (2) (2005) 557–566.
[9] P. Mpofu, J. Addai-Mensah, J. Ralston, Interfacial chemistry, particle interactions and improved dewatering behaviour of smectite clay dispersions, Int. J. Miner. Process. 75 (3–4) (2005) 155–171.
[10] Y. Leong, Surface forces arising from adsorbed hydrolysis products of metal ions in ZrO_2 and silica dispersions: Cu(II), Ni(II), Co(II) and Al(III), Powder Technol. 179 (1–2) (2007) 38–42.
[11] R.M. Pashley, DLVO and hydration forces between mica surfaces in Li^+, Na^+, K^+ and Cs^+ electrolyte solutions: a correlation of double-layer and hydration forces with surface cation exchange properties, J. Colloid Interface Sci. 83 (1981) 531–541.
[12] R.M. Pashley, J.N. Israelachvili, DLVO and hydration forces between mica surfaces in Mg^{2+}, Ca^{2+}, Sr^{2+}, and Ba^{2+} chloride solutions, J. Colloid Interface Sci. 97 (2) (1984) 446–455.
[13] M.V. Maslova, L.G. Gerasimova, W. Forsling, Surface properties of cleaved mica, Kolloidnyj Zh. 66 (3) (2004) 364–371.
[14] J.S. Lyons, D.N. Furlong, T.W. Healy, The electrical double-layer properties of the mica (muscovite)–aqueous electrolyte interface, Aust. J. Chem. 34 (6) (1981) 1177–1187.
[15] R.W. O'Brien, D.W. Cannon, W.N. Rowlands, Electroacoustic determination of particle size and zeta potential, J. Colloid Interface Sci. 173 (2) (1995) 406–418.
[16] Q.D. Nguyen, D.V. Boger, Yield stress measurement for concentrated suspensions, J. Rheol. 27 (4) (1983) 321–349.
[17] Q.D. Nguyen, D.V. Boger, Direct yield stress measurement with the vane method, J. Rheol. 29 (3) (1985) 335–347.
[18] N.J. Alderman, G.H. Meeten, J.D. Sherwood, Vane rheometry of bentonite gels, J. Non-Newton. Fluid 39 (3) (1991) 291–310.
[19] Q.D. Nguyen, D.V. Boger, Measuring the flow properties of yield stress fluids, Annu. Rev. Fluid Mech. 24 (1992) 47–88.
[20] J. Addai-Mensah, J. Ralston, Interfacial chemistry and particle interactions and their impact upon the dewatering behaviour of iron oxide dispersions, Hydrometallurgy 74 (3–4) (2004) 221–231.
[21] B.V. Derjaguin, L. Landau, Theory of the stability of strongly charged lyophobic sols and of the adhesion of strongly charged particles in solutions of electrolytes, Acta Physicochim. (URSS) 14 (1941) 633–662.
[22] E.J. Verwey, J.T.G. Overbeek, Theory of the Stability of Lyophobic Colloids, Elsevier, Amsterdam, 1948.
[23] B.A. Firth, R.J. Hunter, Flow properties of coagulated colloidal suspensions: I. Energy dissipation in the flow units, J. Colloid Interface Sci. 57 (2) (1976) 248–256.
[24] B.A. Firth, R.J. Hunter, Flow properties of coagulated colloidal suspensions: III. The elastic floc model, J. Colloid Interface Sci. 57 (2) (1976) 266–275.
[25] R.M. Pashley, Electromobility of mica particles dispersed in aqueous solutions, Clays Clay Miner. 33 (3) (1985) 193–199.
[26] S. Nishimura, H. Tateyama, K. Tsunematsu, K. Jinnai, Zeta potential measurement of muscovite mica basal plane–aqueous solution interface by means of plane interface technique, J. Colloid Interface Sci. 152 (2) (1992) 359–367.
[27] R.J. Hunter, Zeta Potential in Colloids Science, Academic Press, NY, 1981.
[28] R.O. James, T.W. Healy, Adsorption of hydrolysable metal ions at the oxide–water interface, J. Colloid Interface Sci. 40 (1972) 42–81.
[29] K. Okada, N. Arimitsu, Y. Kameshima, A. Nakajima, K.J.D. MacKenzie, Preparation of porous silica from chlorite by selective acid leaching, Appl. Clay Sci. 30 (2) (2005) 116–124.

[30] C.F. Baes, R.E. Mesmer, The Hydrolysis of Cations, Krieger, Malabar, FL, 1986.
[31] W.B. Jepson, D.G. Jeffs, A.P. Ferris, The adsorption of silica on gibbsite and its relevance to the kaolinite surface, J. Colloid Interface Sci. 55 (2) (1976) 454–461.
[32] E. Kusaka, N. Amano, Y. Nakahiro, Effect of hydrolysed aluminum(III) and chromium(III) cations on the lipophilicity of talc, Int. J. Miner. Process. 50 (4) (1997) 243–253.
[33] W.N. Rowlands, R.W. O'Brien, R.J. Hunter, V. Patrick, Surface properties of aluminum hydroxide at high salt concentration, J. Colloid Interface Sci. 188 (2) (1997) 325–335.
[34] T.W. Swaddle, Silicate complexes of aluminum(III) in aqueous systems, Coord. Chem. Rev. 219–221 (2001) 665–686.
[35] G.A. Parks, The isoelectric points of solid oxides, solid hydroxides, and aqueous complex systems, Chem. Rev. 65 (1965) 177–198.
[36] S.B. Johnson, G.V. Franks, P.J. Scales, D.V. Boger, T.W. Healy, Surface chemistry–rheology relationships in concentrated mineral suspensions, Int. J. Miner. Process. 58 (1) (2000) 267–304.
[37] D. Heath, T.F. Tadros, Influence of pH, electrolyte, and poly(vinyl alcohol) addition on the rheological characteristics of aqueous dispersions of sodium montmorillonite, J. Colloid Interface Sci. 93 (2) (1983) 307–319.
[38] T. Permien, G. Lagaly, Rheological and colloidal properties of bentonite dispersions in the presence of organic compounds: I. Flow behaviour of sodium–bentonite in water–alcohol, Clay Miner. 29 (5) (1994) 751–760.
[39] T. Permien, G. Lagaly, Rheological and colloidal properties of bentonite dispersions in the presence of organic compounds: II. Flow behaviour of Wyoming bentonite in water–alcohol, Clay Miner. 29 (5) (1994) 761–766.
[40] L. Bergström, Hamaker constants of inorganic materials, Adv. Colloid Interface Sci. 70 (1997) 125–169.
[41] J.N. Israelachvili, G.E. Adams, Measurement of forces between two mica surfaces in aqueous electrolyte solutions in the range 0–100 nm, J. Chem. Soc. 74 (1978) 975–1001.
[42] R.G. Horn, D.R. Clarke, M.T. clarkson, Direct measurement of surface forces between sapphire crystals in aqueous solutions, J. Mater. Res. 3 (3) (1988) 413–416.
[43] R.H. French, R.M. Cannon, L.K. DeNoyer, Y.-M. Chiang, Full spectral calculation of non-retarded Hamaker constants for ceramic systems from interband transition strengths, Solid State Ionics 75 (1995) 13–33.
[44] J.M. Fernández-Varea, R. Garcia-Molina, Hamaker constants of systems involving water obtained from a dielectric function that fulfills the f Sum Rule, J. Colloid Interface Sci. 231 (2) (2000) 394–397.
[45] H.D. Ackler, R.H. French, Y.-M. Chiang, Comparisons of hamaker constants for ceramic systems with intervening vacuum or water: from force laws and physical properties, J. Colloid Interface Sci. 179 (2) (1996) 460–469.